Journal of Alloys and Compounds 505 (2010) 808–813

Contents lists available at ScienceDirect

Journal of Alloys and Compounds

journal homepage: www.elsevier.com/locate/jallcom

Structure and magnetic properties of NiZn ferrite/SiO_2 nanocomposites synthesized by ball milling

G. Pozo López[a,b,*], S.P. Silvetti[a,b], S.E. Urreta[a], A.C. Carreras[c]

[a] Facultad de Matemática, Astronomía y Física, Universidad Nacional de Córdoba, Ciudad Universitaria, 5000, Córdoba, Argentina
[b] Instituto de Física Enrique Gaviola – CONICET, Argentina
[c] Instituto de Investigaciones en Tecnología Química – CONICET – UNSL, San Luis, 5700, Argentina

ARTICLE INFO

Article history:
Received 1 December 2009
Accepted 24 June 2010
Available online 3 July 2010

PACS:
75.50.Gg
75.50.Tt
75.60.Ej
75.75.+a
81.20.Ev

Keywords:
NiZn ferrite/SiO_2 nanocomposites
Ball milling
XRD
Magnetic properties

ABSTRACT

Magnetic $NiZnFe_2O_4/SiO_2$ nanocomposites are synthesized by ball-milling a mixture of crystalline α-Fe_2O_3, NiO, ZnO and SiO_2 powders. Crystallographic phases appearing during milling, their particle sizes and lattice parameters are determined from X-ray diffraction (XRD) measurements and the morphology of the as-milled powders observed by scanning electron microscopy (SEM). Room temperature hysteresis properties are characterized by vibrating sample magnetometry. The milling process, up to 260 h, promotes the progressive amorphization of the powders and the formation of different phases, such as NiZn-ferrite, α-Fe and Fe_2SiO_4. For milling times smaller than 80 h, the complete transformation of the precursor oxides into NiZn-ferrite is only achieved after annealing the as-milled powders for 1 h in air at 1273 K. This heat treatment favors the formation of NiZn-ferrite in detriment of the precursor oxides. On the other hand, annealing in air the powder milled 260 h, essentially amorphous, results in the formation of both hematite and NiZn-ferrite in the amorphous silica. When the powders milled for 260 h are heat treated in argon atmosphere, a biphase composite is obtained, with NiZn-ferrite crystallites of about 65 nm dispersed in an amorphous silica matrix. This last powder presents the highest values of saturation magnetization (29.87 Am^2/kg) and coercivity (25.7 kA/m), being the latter two orders of magnitude larger than that of bulk NiZn-ferrite.

1. Introduction

Magnetic composite materials, produced by embedding nanometric magnetic particles in a non-magnetic matrix are intensively investigated because they exhibit novel physical, chemical and electromagnetic properties due to their peculiar structures as compared to those found in bulk materials [1,2]. Among these granular solids, ferrite nanocomposites constitute an important group of materials with interesting technological applications, especially in microwave industries, electronics and telecommunications.

Among the different spinel ferrites, NiZn ferrites are the most versatile magnetic materials for general use. They exhibit low magnetic coercitivity and high electrical resistivity, which greatly reduces eddy current losses at high frequencies, high Curie temperature, good mechanical hardness and chemical stability. Due to all these properties NiZn ferrites have extensive applications such as in recording heads, antenna rods, loading coils, microwave devices, core material for power transformers in electronics and telecommunication applications [3–6].

The traditional methods for preparing ferrites involve conventional solid-state synthesis techniques, which are known to have serious limitations, such as chemical inhomogeneity, poor compositional control and the formation of large particles [7–9]. Several synthesis methods have been developed to prepare ferrite nanoparticles and nanocomposites, including chemical coprecipitation, hydrothermal processing, sol–gel and mechanical alloying. This last technique, in addition to reduce grain size and mix powders uniformly, has proved to be a powerful tool for the synthesis of various kinds of materials, such as amorphous alloys, nanocrystalline metals and alloys and ceramic materials [10,11].

The aims of our work is to describe the mechanical alloying process of precursor oxide powders to obtain a NiZn-ferrite/SiO_2 biphase composite, evaluating the effect of different heat treatments on the powders microstructure and magnetic properties. In this article, we report the synthesis of NiZn ferrite/SiO_2 nanocomposites by a two step process involving: (a) ball milling a mixture of crystalline Fe_2O_3, NiO, ZnO and SiO_2 powders and (b) a subsequent heat treatment at 1273 K, under oxidizing or inert atmosphere.

* Corresponding author at: Facultad de Matemática, Astronomía y Física, Universidad Nacional de Córdoba, Ciudad Universitaria, 5000, Córdoba, Argentina.
Tel.: +54 0351 433 4051; fax: +54 0351 433 4054.
E-mail address: gpozo@famaf.unc.edu.ar (G. Pozo López).

0925-8388/$ – see front matter © 2010 Elsevier B.V. All rights reserved.
doi:10.1016/j.jallcom.2010.06.145

2. Experimental

The starting materials for ball milling are crystalline powders of α-Fe_2O_3 (hematite or α-phase) (99.5% purity), ZnO (99.5% purity), NiO (99% purity) and SiO_2 (99% purity), commercially available and with an average particle size of about 200 nm. A mixture of these materials with the proportion: 50 wt% SiO_2 + 24.75 wt% Fe_2O_3 + 21.45 wt% NiO + 3.79 wt% ZnO is chosen as precursor powder. The milling operation is carried out at room temperature, under air atmosphere without any additives, in a planetary ball milling device (Fritsch Pulverisette 5), equipped with hardened stainless steel vials and balls. The initial ball to powder mass ratio is 10:1. The powder is milled at a speed of 200 rpm for milling times from 1 h to 260 h. Then, the powders are heat treated to reduce the internal strain introduced by the milling process and to promote the formation of the desired compound.

The mechanochemical reaction is monitored by X-ray diffraction (XRD) analysis. Small quantities of powder are taken out from the vial every 10 h grinding for X-ray diffraction analysis and magnetic measurements. The corresponding milled samples are labeled Mm, where "*m*" is the milling time, in hours. Furthermore, the powders milled for 30, 60, 80 and 260 h are subsequently heat-treated for 1 h at 1273 K in air. Powders milled for 260 h are also heat treated under argon atmosphere.

X-ray diffraction (XRD) spectra are measured in a Philips PW 3830 diffractometer, using Cu Kα radiation (λ = 1.5418 Å) and they are recorded for a 2θ range between 10° and 100°, at a scanning speed of 1.2°/min. A profile fitting is made for each maximum in the spectra to determine the peak width, after correcting for instrumental broadening. XRD is used to identify the different crystalline phases in the samples as well as to estimate their lattice parameters and average grain sizes.

A LEO 1450 VP scanning electron microscope (SEM) is used to characterize the size and morphology of powder particles. X-ray fluorescence (XRF) analysis is performed with a Philips PW 1400 wavelength-dispersive X-ray spectrometer. Samples are irradiated with incident X-rays from a rhodium tube operated at 30 kV and 30 mA. Spectra are measured in step scan mode with a PET (2*d* = 8.742 Å) crystal analyzer.

Magnetization measurements are performed on samples prepared by cold-pressing the powders in a 5 ton-press, into cylinders of 6.5 mm diameter and typically 2 mm height. Room temperature magnetization curves are measured in a vibrating sample magnetometer (VSM) Lakeshore 7300, with a maximum field up to 1.5 T. The applied field is corrected by the demagnetizing field – a geometric demagnetizing factor of 0.2 is assumed – to calculate the internal field H_i. The evolution of the saturation magnetization (M_S), the remanent magnetization (M_R) and the coercive field ($H_{iC} = H_i(M = 0)$) of the as-milled and annealed powders is investigated. Saturation magnetization values are obtained by fitting the high field data ($H_i > 1.2$ T) to the function $M = M_S\,(1 - \alpha/H_i)$ [12], where M_S is the saturation magnetization of the composite, α is a measure of the magnetic hardness and H_i is the internal magnetic field.

3. Results and discussion

3.1. Effect of ball-milling

Fig. 1 shows the diffraction profiles of the powder after 0, 60, 80, 100, 140 and 260 h of milling operation. After ball-milling for 60 h, significant line-broadening of the precursor oxide peaks is clearly observed, indicating a drastic grain size refinement. The main consequences of milling are the dissolution of the initial oxides and the apparition of NiZn-ferrite. Since there is no significant difference between XRD patterns of the powder milled for times shorter than 60 h, these conditions are not further investigated. M60 XRD profile shows NiZn-ferrite, with the (3 1 1), (4 0 0) and (4 4 0) peaks clearly defined in Fig. 1; in these samples, the intensity of diffraction peaks due to α-Fe_2O_3, NiO and SiO_2 are reduced and the peaks from ZnO disappear. Subsequent milling up to 80 h increases the proportion of spinel NiZn-ferrite and promotes the formation of small α-Fe grains, whereas the peaks corresponding to the precursor oxides practically vanish. Further milling modifies the ferrite peak position and width, indicating that lattice parameter and grain size also change. After 100 h milling the amorphization process is more evident. The most intense line of BCC Fe (1 1 0) is observed between 80 h and 140 h milling. Besides, another new crystalline phase appears, as an intermediate product, during the milling between 120 h and 200 h. The corresponding new peaks are located at 2θ angles of 25.0°, 31.7° and 51.5°, and they are identified as arising from the Fe_2SiO_4 (fayalite) phase. The diffraction pattern of the powder milled up to 260 h shows a few, very broad peaks, attributed to NiO, and a broad halo over the range 30–40°, characteristic of amorphous phases. At this stage, the most intense reflection from alpha-quartz (1 0 1) completely disappears and the sample consists of magnetic nanocrystallites embedded in an amorphous matrix.

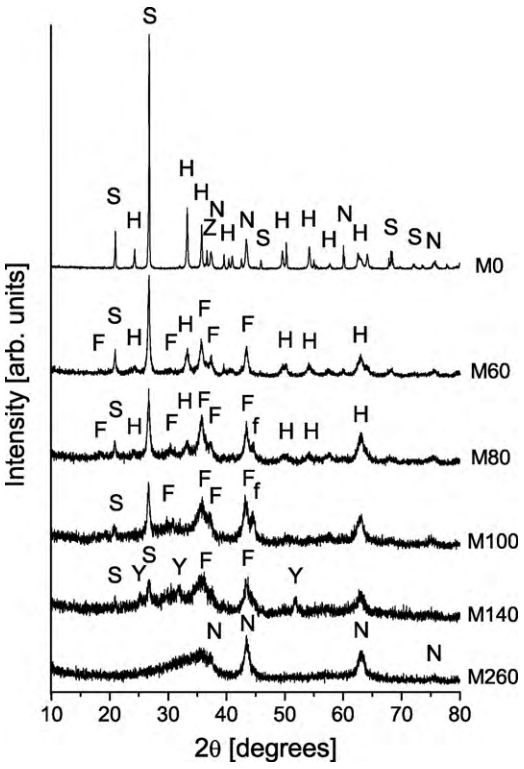

Fig. 1. X-ray diffraction patterns of the powders as a function of milling time. The principal diffraction lines of the precursor oxides: hematite (H), nickel oxide (N), zinc oxide (Z) and quartz (S), and the ones corresponding to the phases formed during milling: NiZn-ferrite (F), α-Fe (f) and fayalite (Y), are also presented.

The average crystallite size *D* of the as-milled mixtures is monitored as a function of milling time. These results are shown in Fig. 2a. The average crystallite size of the different phases is estimated by means of the Scherrer equation [13,14]: $D = (0.9\lambda)/(\mathrm{FWHM}_i \cos\theta)$, where FWHM_i is the full-width at half-maximum of the diffraction peak, in radians, after subtraction of the instrumental contribution; λ is the X-ray wavelength and θ_i is the diffraction angle. In the present case, the reflections used for each phase are: (2 2 0) for NiZn-ferrite, (1 0 4) for hematite, (1 0 1) for SiO_2, (1 1 0) for α-Fe and (2 2 2) for fayalite. In all the cases the values of *D* are estimated with incertitude of about 5 nm. The evolution of the crystallite size is followed up to 140 h milling, as for larger times it was very difficult to determine the width and position of the different peaks due to amorphization. In the case of hematite and NiZn ferrite phases, the analysis was stopped at earlier milling times due to reflection line overlapping from different phases, in addition to amorphization. Fig. 2a shows that D_{quartz} continuously decreases, from approximately 200 nm to 19 nm after 140 h milling. The same behavior is observed for the other phases, which decrease their average crystallite size with the milling time: D_{hematite} is found to decrease from 54 nm to about 14 nm after 80 h milling; D_{ferrite} presents values from 15 nm in sample M60 to ~6 nm in sample M120. On the other hand, D_{Fe} and D_{fayalite} exhibit a small variation during milling in the time interval observed, taking values from 12 nm to 9 nm in the case of Fe and about 15 nm for fayalite.

The mean lattice strain e is determined using the Stokes and Wilson relation [14]: $e = (\beta/4)\cot\theta$, from measurements of the integral breath β of the reflection lines. Fig. 2b illustrates the evolution of the lattice strain of the different crystalline phases detected in the powder during milling. It may be observed that the mean lattice

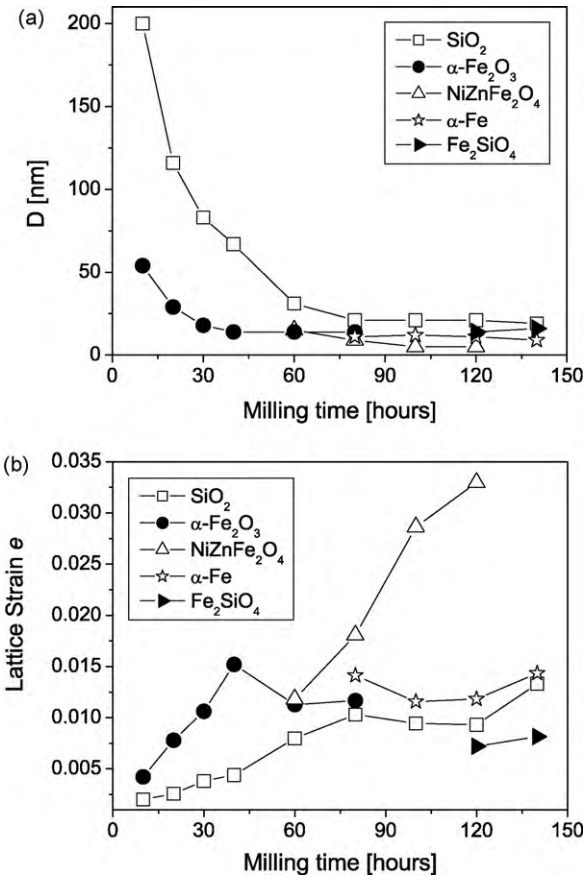

Fig. 2. Average crystallite size D (a) and mean lattice strain e (b) as functions of the milling time, for the crystalline phases detected in the samples.

strain of the different phases increase with the milling time. This behavior is commonly observed in mechanical alloying: the grain size decreases while the lattice strain increases with the milling time. e_{hematite} presents a small reduction when NiZn ferrite phase is first detected by XRD after 60 h milling. On the other hand, the values of e_{Fe} do not exhibit any important variation during milling, as it is a ductile phase immersed in a mainly ceramic matrix.

SEM micrographs of samples M30 and M260 – shown in Fig. 3 – illustrate the resulting powder grains. These powder grains are agglomerates of smaller particles with mean size of about 500 nm in M30 and 100 nm in M260. The agglomerates are somewhat larger in M260 as a result of welding during grinding. The external morphologies of powders M30 and M260 are quite similar even though the former is completely crystalline while the latter is essentially amorphous.

The evolution of room temperature magnetic properties during milling is summarized in Fig. 4. It may be observed that saturation magnetization (M_S) is almost constant until 40 h milling, when only the initial oxides (NiO: antiferromagnetic, ZnO: paramagnetic and α-Fe_2O_3: weakly ferromagnetic) are present. After 40 h milling, M_S rapidly increases, reaching the highest value for sample M80 (13.4 Am^2/kg). This occurs at the same time that the crystalline structure is changing to form the NiZn-ferrite as a new magnetic phase. From 80 h milling, M_S diminishes because the crystalline structure of NiZn-ferrite progressively deteriorates, as revealed by X-ray diffraction analysis (at that point the sample begins to amorphize) and during further milling, due to the formation of paramagnetic fayalite. From 140 up to 260 h of ball-milling, M_S remains almost constant, while the sample becomes nominally amorphous (amorphous for XRD) except for the NiO reflections, which are clearly visible. After 260 h milling, the powders do not

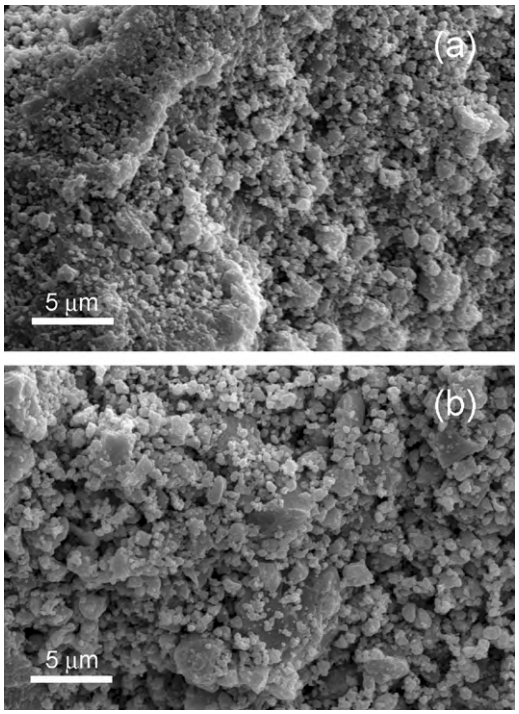

Fig. 3. SEM secondary electrons micrographs of milled samples for (a) 30 h and (b) 260 h.

saturate, indicating that in addition to the ferromagnetic contribution, a paramagnetic or super-paramagnetic one is also present. The remanence behaves in a similar manner to the saturation magnetization, reaching its highest value, of about 1.6 Am^2/kg, in sample M80.

Coercivity (H_{iC}) first increases during 60 h milling, reaching at this time its maximum of 17 kA/m. From this time and up to 140 h of ball-milling, H_{iC} continuously decreases as a consequence of progressive amorphization. According to XRD results, the magnetic phases present in the samples at this time are NiZn-ferrite and BCC Fe, both with nanometer size ($\leq$10 nm). Then, these small grains are in a super-paramagnetic state leading to the diminution of coercivity with longer milling times. The smallest value of H_{iC} is reached after 140 h milling and is about 6 kA/m. For long-term milling (from 140 h to 200 h) coercivity again increases, reaching a quite stable value after milling for 200 h. This magnetic hardening, taking place at an almost constant value of M_S, is likely to arise in the exchange coupling between the small ferromagnetic ferrite particles and the also small antiferromagnetic NiO parti-

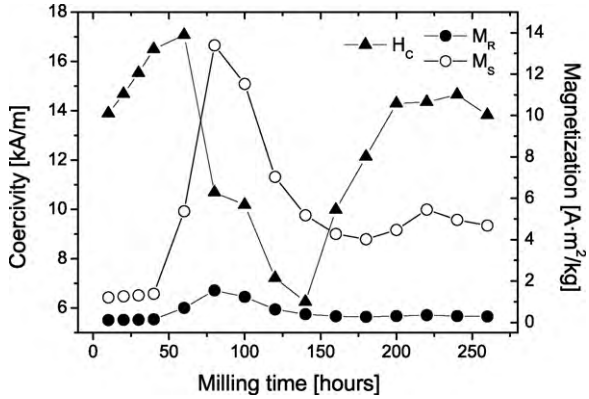

Fig. 4. Room temperature saturation magnetization M_S, remanence M_R and coercivity H_C as a function of milling time.

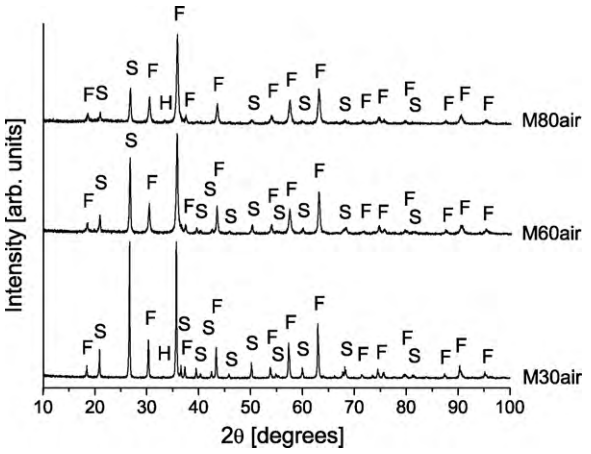

Fig. 5. X-ray diffraction patterns of the powders milled 30, 60 and 80 h and heat treated at 1273 K for an hour in air atmosphere. The principal diffraction lines of α-quartz (SiO_2—S), NiZn-ferrite ($NiZnFe_2O_4$—F) and hematite (α-Fe_2O_3—H) are also shown.

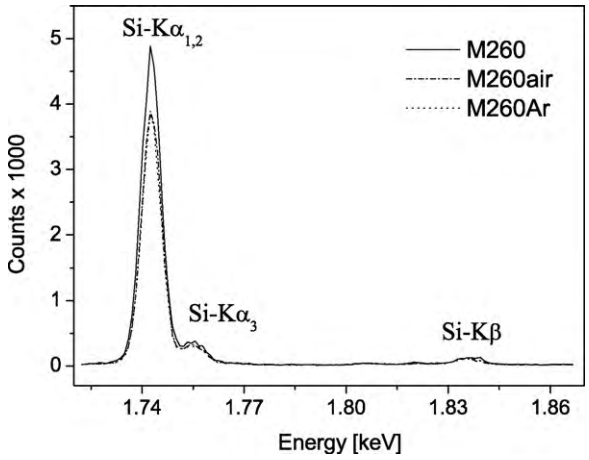

Fig. 7. X-ray fluorescence spectra of Si for the powders milled 260 h (M260) and further annealed at 1273 K for 1 h in air (M260air) and argon (M260Ar) atmosphere.

cles. Enhancements in coercivity, squareness and energy product have been obtained at room-temperature by mechanically milling mixtures of ferromagnetic (FM) and antiferromagnetic NiO [15,16] powders.

3.2. Effect of heat treatments

Samples milled for 30, 60, 80 and 260 h are then heat treated at 1273 K for 1 h in air atmosphere to study the crystallization behavior. The samples milled up to "*m*" hours and annealed in air atmosphere are named M*m*air.

The XRD results for the annealed samples are presented in Figs. 5 and 6. As can be seen in Fig. 5, very similar patterns are obtained for samples M30air, M60air and M80air. The differences are mainly related to changes in the relative peak intensities and to the fact that for higher milling times the proportion of crystalline SiO_2 in the sample is smaller. The XRD results show that this heat treatment favors the formation of NiZn-ferrite phase, and contributes to the disappearance of the α-Fe_2O_3 peaks in the corresponding diffraction patterns. The phases present after the heat treatments are mostly NiZn-ferrite and crystalline SiO_2, with small traces of α-Fe_2O_3

The situation is different in the case of sample M260air, shown in Fig. 6. XRD analysis of this sample reveals that after the heat treatment, the major phases are hematite and NiZn-ferrite. Traces of NiO can also be detected. No other crystalline phases are observed in the pattern, indicating that SiO_2 is now dispersed as an amorphous phase. The presence of α-Fe_2O_3 in the sample M260air may be explained by considering that for the heat treatment at 1273 K, the temperature is high enough to produce a fast oxidation of free iron to hematite. In order to obtain information about the oxidation of Fe to α-Fe_2O_3, the powder milled 260 h (M260) is heat treated at 1273 K for 1 h in argon atmosphere (sample M260Ar). The corresponding XRD pattern is also included in Fig. 6. Sample M260Ar has a different structure and the only crystalline phase observed after transformation is NiZn-ferrite. No other crystalline phases are found and no traces of quartz, cristobalite nor intermediate products involving silicon (e.g. Fe_2SiO_4) are detected, indicating that the silicon oxide present in the samples is nominally amorphous for XRD. Thus, most of the nanocrystalline ferrite formed in the amorphous silica matrix.

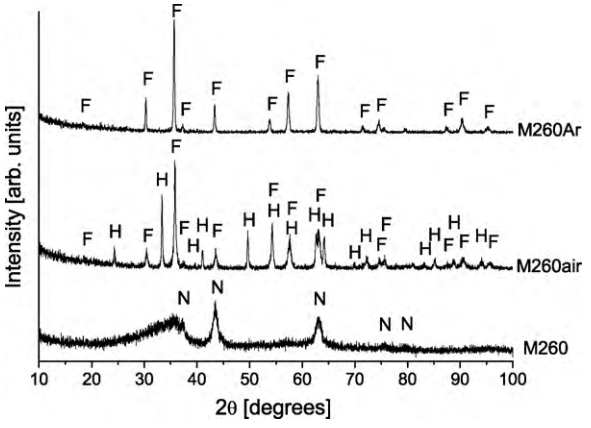

Fig. 6. X-ray diffraction patterns of the powders milled 260 h (sample M260) and annealed at 1273 K for an hour in air (sample M260air) and argon atmosphere (sample M260Ar). The principal diffraction lines of NiZn-ferrite (F), hematite (H) and nickel oxide (N) are also shown.

The presence of silica in samples M260, M260air and M260Aar is further corroborated by XRF analysis. Fig. 7 shows the measured X-ray fluorescence spectra of Si for the powders both, as milled and after the heat treatments at 1273 K. As can be observed, all the samples exhibit silicon peaks, being the annealed samples spectra almost identical.

It is well known that the magnetic properties of ferrites are influenced by chemical composition and by the actual crystal microstructure, including grain size, grain boundaries, porosity, atomic defects and structural homogeneity. The magnetic properties of ferrite composites are mainly determined by the ferrite content and its average grain size [1]. The average crystallite size of NiZn-ferrite, as determined from XRD analysis through the (3 1 1) reflection for samples milled and further annealed and the (2 2 0) reflection for the as-milled samples (the latter due to peak overlapping with hematite reflections) are shown in Table 1, together with the room temperature magnetic parameters of the composites. It should be noted that the mean ferrite crystallite size is almost constant (around 30 nm) for samples M60air, M80air and M260air, while it exhibits a much higher value in the case of sample M30air, of about 110 nm. In this sample, NiZn-ferrite is formed during the heat treatment at 1273 K because there are no observable traces of this phase in the as-milled M30 sample. On the other hand, samples M60 and M80 already present a fraction of NiZn-ferrite phase formed during the milling process and sample M260 is essentially amorphous with nanocrystalline (<10 nm) NiO and/or NiZn ferrite small particles, non detected by XRD. The main difference between all these samples is that the heat treatment in air atmosphere favors the formation of NiZn-ferrite at expenses of hematite in samples

Table 1
Lattice constant a and mean crystal size D for the NiZn-ferrite phase obtained from XRD data for the samples milled and annealed in different atmospheres. Also included are the room temperature coercive field H_{iC}, saturation magnetization M_S and the remanent magnetization M_R of the nanocomposites investigated.

Sample	a [Å]	D [nm]	H_{iC} [kA/m]	M_S [Am^2/kg]	M_R [Am^2/kg]
M30	–	–	15.5	1.31	0.13
M30air	8.349	110	10.9	27.70	5.74
M60	8.363	15	17.1	5.37	0.70
M60air	8.347	35	11.2	22.68	4.03
M80	8.343	9	10.7	13.39	1.55
M80air	8.349	34	6.4	26.94	4.30
M260	–	–	13.8	4.68	0.29
M260air	8.342	32	5.8	17.97	4.26
M260Ar	8.348	65	25.7	29.87	11.00

M30air, M60air and M80air, but it promotes oxidation with the formation of both hematite and NiZn-ferrite in sample M260air, as was already mentioned.

Sample M260Ar shows a different microstructure. It is composed by NiZn-ferrite as the only crystalline phase, with an average particle size of 65 nm. NiZn-ferrite lattice constant a obtained from the XRD profile fitting is also presented in Table 1. The values of a around 8.344 Å obtained for most of the samples are consistent, within experimental errors, with a crystalline structure of $Ni_{0.8}Zn_{0.2}Fe_2O_4$ [17]. The only sample that deviates from this tendency is M60, whose lattice constant, equal to 8.363 Å, implies a lower nickel content, of about 0.6 [17].

The room temperature $M(H)$ curves for samples M30, M60 and M80 and their corresponding heat-treatments in air atmosphere at 1273 K are shown in Fig. 8; the magnetic parameters, derived from these loops, are also resumed in Table 1. It is seen that M_S and H_C values change as a consequence of heat-treatment. The saturation magnetization has increased in the three heat-treated samples with respect to the non-treated ones. Owing to the fact that the saturation magnetization is only related to the nature and the volume fraction of magnetic particles in the sample, the changes are attributed to the apparition of the ferrimagnetic NiZn-ferrite phase. The saturation magnetization increases with the ferrite content due to an increase in the number of magnetic dipoles in the unit volume [1,18].

Magnetization curves obtained for samples M260air and M260Ar are shown in Fig. 9, together with the hysteresis loop of M260 for comparison. The saturation magnetization values in this case are 17.97 Am^2/kg for the sample heat-treated in air and 29.87 Am^2/kg for the sample annealed in argon atmosphere. Such differences can be explained taking in consideration that M260air is mainly composed of amorphous silica (diamagnetic) and crystalline hematite (weakly ferromagnetic), so the observed magnetization of the composite only corresponds to the NiZn-ferrite present in it (<25 wt%). On the other hand, the sample heat-treated in argon consists of crystalline NiZn-ferrite (50 wt%) dispersed in an amorphous silica matrix. For this last sample, the specific saturation magnetization M_S of the ferrite phase, calculated from the saturation magnetization of the composite M_S, results in 59.74 Am^2/kg, a value that is smaller than the saturation magnetization for bulk NiZn-ferrite (67.2 Am^2/kg [19,20]). This phenomenon of a reduced saturation magnetization has already been reported for NiZn-ferrite nanoparticles [6,21,22] and NiZn-ferrite/SiO_2 nanocomposites [2,23], synthesized by different physical and chemical techniques, and may be ascribed to surface or finite size effects of the nanoparticles, i.e. a reduction in the exchange coupling in the surface causing spin canting [24].

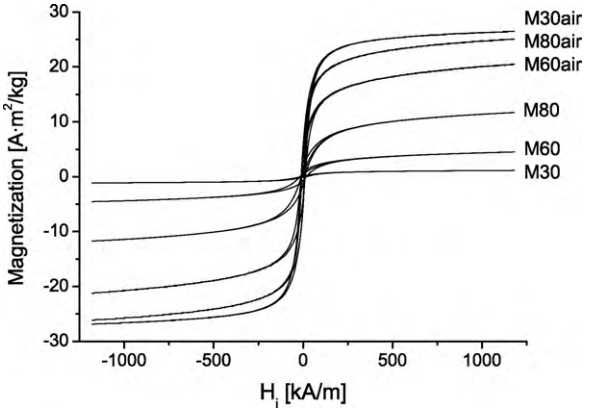

Fig. 8. Room temperature hysteresis loops for samples milled up to 30, 60 and 80 h and further heat-treated in air at 1273 K during 1 h.

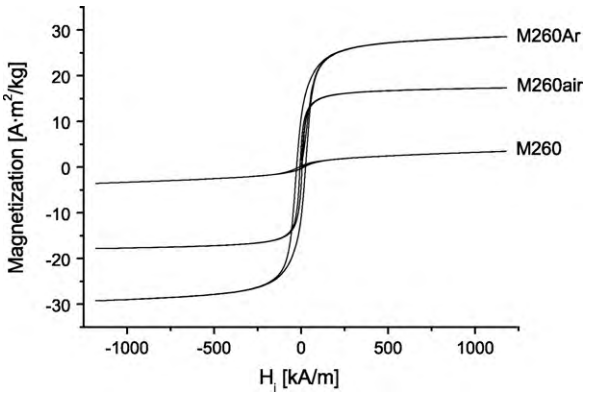

Fig. 9. Room temperature hysteresis loops for samples milled up to 260 h and further heat-treated in air and argon atmosphere, at 1273 K during 1 h.

The coercivity in these samples also depends of the atmosphere used in the heat treatment, resulting in 5.8 kA/m for sample M260air and 25.7 kA/m for sample M260Ar. This last value of H_{iC} is the highest one obtained in this work and is near two orders of magnitude higher than the corresponding value for bulk NiZn-ferrite [17] and almost three times higher than the coercivity measured for a similar NiZn-ferrite/SiO_2 nanocomposite synthesized by sol–gel processing [25]. This high value of coercivity in sample M260Ar is attributed to an increase of the mean size of the NiZn-ferrite crystallites embedded in the amorphous silica matrix, as compared to samples M80air and M60air. In all these cases, the magnetic particles have a mean size smaller than the critical single domain diameter, so reversion mechanisms involving more or less uniform polarization rotation are expected, which lead to a coercivity increasing with the mean particle volume. For the NiZn-ferrite powders synthesized in this work the critical single domain diameter is between 65 nm and 110 nm. Samples with larger crystal sizes show small coercivity values, around 11 kA/m, indicating that domain-wall displacement is dominant in the magnetization process. This critical single domain size (110 nm) is largely smaller than the micrometer size observed for bulk NiZn-ferrite samples [26] but a little higher than the values around 30–40 nm obtained for NiZn-ferrite powders synthesized by chemical methods [27,21].

4. Conclusions

In this work NiZn-ferrite/silica nanocomposites are obtained by ball-milling a mixture of crystalline of α-Fe_2O_3, NiO, ZnO and SiO_2 powders. The main effect of grinding is the apparition of various phases at different stages of milling, such as NiZn-ferrite, α-Fe and Fe_2SiO_4 (fayalite) and a long term powder amorphization.

Magnetic properties are sensitive to these microstructure changes; at the beginning the saturation magnetization grows due to the gradual apparition of NiZn-ferrite (ferrimagnetic) and then after 100 h milling it decays due to the formation of fayalite (paramagnetic) and amorphization. Three different coercivity regimes are identified during the milling process: a slight increase in H_{iC} until 60 h milling (multidomain regime, diminution of grain size), followed by a decrease until 140 h milling (single domain regime, diminution of grain size) and finally another increase in the coercive field, associated to exchange hardening of the ferromagnetic phase by small NiO antiferromagnetic particles.

A complete transformation of the precursor oxides into NiZn-ferrite is not achieved by solely ball-milling the precursor powder for 30, 60 and 80 h; further annealing of these powders for 1 h at 1273 K in air atmosphere is necessary to form NiZn-ferrite at expenses of the remanent precursor oxides. The samples annealed consist of crystalline NiZn-ferrite and SiO_2, in addition to small quantities of residual hematite. The average crystallite size for NiZn-ferrite in these samples is 110, 35 and 34 nm, for M30air, M60air and M80air respectively. Additional heat treatments are performed for powders milled up to 260 h in air and argon atmospheres. In this case, annealing in air promotes the sample oxidation, resulting in the formation of both hematite and NiZn-ferrite almost in the same proportion. On contrary, annealing in argon atmosphere results in a biphase nanocomposite consisting of 65 nm-NiZn-ferrite particles dispersed in an amorphous SiO_2 matrix. Saturation magnetization and coercivity reached their highest values for this sample, of about 29.87 Am^2/kg and 25.7 kA/m, respectively.

Acknowledgments

The authors wish to thank CONICET, Agencia Córdoba Ciencia and SECyT-UNC the financial support given for the realization of this work.

References

[1] X. He, Q. Zhang, Z. Ling, Mater. Lett. 57 (2003) 3031–3036.
[2] M. Stefanescu, M. Stoia, C. Caizer, O. Stefanescu, Mater. Chem. Phys. 113 (2009) 342–348.
[3] J.B. da Silva, N.D.S. Mohallem, J. Magn, Magn. Mater. 226–230 (2001) 1393–1396.
[4] A.C.F.M. Costa, E. Tortella, M.R. Morelli, R.H.G.A. Kiminani, J. Magn. Magn. Mater. 256 (2003) 174–182.
[5] M. Jalaly, M.H. Enayati, F. Karimzadeh, J. Alloys Compd. 480 (2009) 737–740.
[6] M. Sertkol, Y. Köseoğlu, A. Baykal, H. Kavas, A.C. Başaran, J. Magn. Magn. Mater. 321 (2009) 157–162.
[7] A.C.F.M. Costa, M.R. Morelli, R.H.G.A. Kiminani, Cerâmica 49 (2003) 133–140.
[8] P.S. Anil Kumar, J.J. Shrotri, S.D. Kulkami, C.E. Deshpande, S.K. Date, Mater. Lett. 27 (1996) 293–296.
[9] A. Verma, T.C. Goel, R.G. Mendiratta, P. Kishan, J. Magn. Magn. Mater. 208 (2000) 13–19.
[10] Č. Jovalekić, M. Zdujić, A. Radaković, M. Mitrić, Mater. Lett. 24 (1995) 365–368.
[11] L. Yu, J. Zhang, Y. Liu, C. Jing, S. Cao, J. Magn. Magn. Mater. 288 (2005) 54–59.
[12] B.D. Cullity, Introduction to Magnetic Materials, Addison-Wesley, Reading, MA, 1972.
[13] H. Klug, L. Alexander, X-Ray Diffraction Procedures for Polycrystalline and Amorphous Materials, second ed., John Wiley and Sons, 1974.
[14] S. Vives, E. Gaffet, C. Meunier, Mater. Sci. Eng. A366 (2004) 229–238.
[15] J. Nogués, I.K. Schuller, J. Magn. Magn. Mater. 192 (1999) 203–232.
[16] J. Sort, J. Nogués, X. Amils, S. Surinñach, J.S. Muñoz, M.D. Baro, J. Magn. Magn. Mater. 219 (2000) 53–57.
[17] J. Smit, H.P.J. Wijn, Ferrites, Physical Properties of Ferrimagnetic Oxides in Relation to their Technical Applications, Philips Technical Library, 1959.
[18] A. Dias, R.L. Moreira, N.D.S. Mohallem, A.I.C. Persiano, J. Magn. Magn. Mater. 172 (1997) L9–L14.
[19] R.C. O'Handley, Modern Magnetic Materials. Principles and Applications, John Wiley and Sons, 2000.
[20] K.H.J. Buschow, F.R. de Boer, Physics of Magnetism and Magnetic Materials, Kluwer Academic/Plenum Publishers, New York, 2003.
[21] H.E. Zhang, B.F. Zhang, G.F. Wang, X.H. Dong, Y. Gao, J. Magn. Magn. Mater. 312 (2007) 126–130.
[22] S. Thakur, S.C. Katyal, M. Singh, J. Magn. Magn. Mater. 321 (2009) 1–7.
[23] G. Pozo López, S.P. Silvetti, M.del C. Aguirre, A.M. Condó, J. Alloys Compd. 487 (2009) 646–652.
[24] R.H. Kodama, A.E. Berkowitz, E.J. McNiff, S. Foner Jr., J. Appl. Phys. 81 (1997) 5552–5557.
[25] A.S. Albuquerque, J.D. Ardisson, E. Bittencourt, W.A.A. Macedo, Mater. Res. 2 (1999) 235–238.
[26] A. Aharoni, J.P. Jacubovics, J. Phys. IV France 08 (1998) 389–392.
[27] A.S. Albuquerque, J.D. Ardisson, W.A.A. Macedo, J. Appl. Phys. 87 (2000) 4352–4357.